

In-situ synchrotron energy-dispersive x-ray diffraction study of thin Pd foils with Pd:D and Pd:H concentrations up to 1:1

D. L. Knies,¹ V. Violante,² K. S. Grabowski,¹ J. Z. Hu,³ D. D. Dominguez,¹ J. H. He,⁴ S. B. Qadri,^{1,a)} and G. K. Hubler¹

¹*U.S. Naval Research Laboratory, Washington, DC 20375, USA*

²*ENEA, Frascati, Italy*

³*NSLS, Brookhaven National Laboratory, Brookhaven, New York 11973, USA*

⁴*Nova Research, Alexandria, Virginia 22308, USA*

(Received 13 July 2012; accepted 19 September 2012; published online 18 October 2012)

Time resolved, *in-situ*, energy dispersive x-ray diffraction was performed in an electrolysis cell during electrochemical loading of palladium foil cathodes with hydrogen and deuterium. Concentrations of H:Pd (D:Pd) up to 1:1 in 0.1 M LiOH (LiOD) in H₂O (D₂O) electrolyte were obtained, as determined by both the Pd lattice parameter and cathode resistivity. In addition, some indications on the kinetics of loading and deloading of hydrogen from the Pd surface were obtained. The alpha-beta phase transformations were clearly delineated but no new phases at high concentration were determined. © 2012 American Institute of Physics.

[<http://dx.doi.org/10.1063/1.4759166>]

INTRODUCTION

Since the discovery in 1886 by Graham¹ that Pd can absorb relatively large amounts of hydrogen, palladium hydrides and deuterides have been extensively studied. Metal hydrides have generated much interest among a variety of scientific disciplines, particularly in hydrogen storage in recent years,^{2,3} because of the limited supply of fossil fuels and growing worldwide demand for energy. Palladium and its alloys are also materials extensively used for hydrogen purification,⁴ which is applicable to fuel cells. Although current research on hydrogen storage has shifted from transition metals to light elements to gain a high gravimetric density of hydrogen, palladium still plays an important role in the study of metal hydrides. The phase diagram of Pd-H shows this system to have two phases, α and β , separated by a miscibility gap for temperatures below about 300 °C and a hydrogen pressure below about 20 bars. At room temperature, the solubility limit for H in the dilute α phase is about 0.03 H/Pd, while the lower limit for the concentrated β phase is 0.58 H/Pd. In between is a two-phase region with a mixture of α and β at these H concentration limits. Both α and β are FCC interstitial solid solutions, but with different lattice parameters. In both, hydrogen atoms randomly occupy the four octahedral interstitial sites present per FCC unit cell containing four palladium atoms. So, when fully loaded with H, stoichiometric PdH forms the B1, or rocksalt structure. The Pd lattice parameter increases from 3.889 Å for pure Pd up to 4.102 Å for PdH at room temperature, an increase over 5.5%. However, deviations from this simple structural model have been reported. For nanocrystalline palladium, a narrowing of the Pd-H miscibility gap has been observed using *in-situ* synchrotron x-ray diffraction (XRD) measurements.⁵ The phase boundary change is associated with a larger ratio of the value of the entropy of mixing to that of the enthalpy

of mixing in nanocrystalline samples than in coarse-grained samples. At low temperature (50–80 K) in the concentrated β phase of PdH, there is the so-called 50-K anomaly, associated with a structure change.⁶ At high hydrogen pressures, a hydrogen-induced superabundant-vacancy phase can be produced in the palladium metal lattice⁷ and stabilized at room temperature and normal pressure.⁸

At high H (D) concentrations, there is some evidence for additional structure changes. Tripodi *et al.* suggested a new γ phase to explain the temperature coefficient of resistance (TCR) increase for electrochemically loaded palladium when the composition H/Pd approached one.⁹ Recently, they showed the TCR decreases when H/Pd exceeds one.¹⁰ In the Pd-D system, new phases were reported from deuterium thermal desorption spectra taken from Pd samples.¹¹ In addition, there was a report showing oscillating resistivity for palladium hydrides at a high concentration range of H/Pd > 0.9.¹²

All these recent experiments suggest that something must happen in palladium with a ratio of H/Pd approaching unity or above, which is currently not understood. Moreover, these proposed phase transitions are only based on indirect experimental data and have not been structurally determined yet. In fact, while loadings of H and D approaching 1:1 D:Pd and H:Pd have been measured *in situ* at 77 K on Pd powder¹³ the highest loading of D/Pd that has been measured at room temperature by *in-situ* x-ray diffraction is 0.76.^{14,15} For these reasons, we have undertaken this *in situ* XRD investigation of Pd highly loaded with H and D at near room temperature.

EXPERIMENTAL PROCEDURE

Fig. 1 shows a schematic representation of the experimental geometry used with the wiggler beam line X17C at the National Synchrotron Light Source, Brookhaven National Laboratory. A collimated, high-intensity, white-radiation x-ray beam with energies of 10–100 keV entered from the left

^{a)}Email: qadri@anvil.nrl.navy.mil.

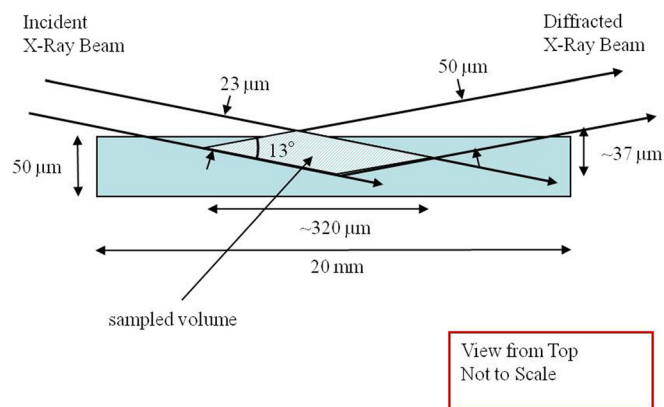


FIG. 1. Schematic representation of experimental geometry used. Beam widths collimated to dimensions shown, with an incident beam height of 12–15 μm , resulting in a sampled volume of ~ 70 pl, with maximum dimensions as shown. A high resolution Ge detector was positioned at a diffraction angle of $2\theta = 13^\circ$.

and impinged upon the center of a sample stage that provided x-y-z translation and two axes of rotation, ω for the sample and 2θ for the detector. The incident x-ray beam was collimated to a shape 12–15 μm tall and 23 μm wide. The diffracted beam was collimated to 50 μm width by tungsten slits, and detected by a high resolution Ge x-ray detector. Nominally symmetric reflection diffraction conditions were used with $\omega \approx 1/2 2\theta = 6.5^\circ$, meaning grazing incidence and a shallow sampling volume applied. As a guide, the x-ray path length in Pd is almost 18 times its depth of penetration with this geometry. For energies just above the Pd K absorption edge at 24.35 keV, the short absorption length in Pd (i.e., $1/\mu$) of about 14 μm limits sensitivity to depths very near the surface. Just below the Pd K edge and up at 47 keV, $1/\mu$ is 83 μm , allowing sensitivity to the top 10 or so μm of the foil. Only for energies >80 keV (where $1/\mu = 335 \mu\text{m}$) is the entire thickness of the foil accessible, as selected by positioning the sampling volume within the foil. We employed the Pd K_{α} x-ray fluorescence at 21.13 keV ($1/\mu = 55 \mu\text{m}$) to position the

sample surface in the diffraction sampled volume, based on the intensity of this x-ray fluorescence. Diffraction data from high energy x-rays were sometimes obtained even when the Pd K x-ray was not observed, because it would be totally absorbed by the cathode at depths greater than $\sim 30 \mu\text{m}$ ($10 \times 1/\mu \div 18$). The original Pd grain size of the cathodes averaged 100 μm , so that most spectra sampled a mixture of two or three grains that the sampled volume straddled during the measurement.

The 2θ diffraction angle was set to 13° to transmit the x-ray beam between the cathode and anode, and to enable diffraction from a broad range of d spaces. The diffraction angle was calibrated using a gold target substituted for the cell. The experimental procedure was to take x-ray spectra prior to beginning electrolysis, and to also establish the starting resistance to enable measurement of R/R_0 , where R is the measured resistance and R_0 is the starting value. The x-y-z stage and ω were used to align the cathode within the sampled volume and to establish the Bragg diffraction condition.

The electrochemical cell, fabricated at ENEA, consisted of a 26-mm-OD glass tube with 1-mm-thick walls and an electrolyte volume of 25 ml. The x-rays passed through the glass wall and about 12 mm of electrolyte to reach the cathode and another 12 mm of electrolyte and the glass wall before emerging from the cell. This limited the detection of diffracted x-rays to energies greater than ~ 20 keV. The cathode was positioned at the center of rotation of the sample stage and initial alignment was performed with a microscope. The parallel-plate, dual-anode-geometry electrochemical cell is illustrated in Fig. 2. The two anodes were 50- μm -thick Pt foils and the cathodes were nominally 50- μm -thick Pd foils. All electrodes were 20 mm wide and 40 mm in height. The anodes and cathode were separated by 4-mm-thick Teflon spacers, used to clamp the electrodes together at each end. Five Pt wires were spot-welded to the Pd foil: one contact for the cathode current and four for the four-point probe measurement of resistivity at a frequency of 1 kHz. Initial resistance of the Pd was a few m Ω . The cell was hermetically sealed,

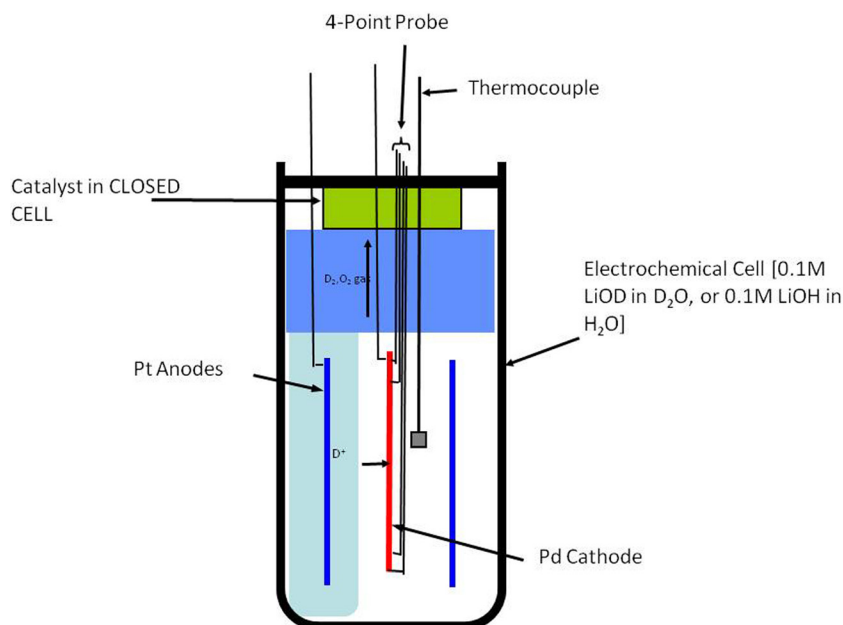


FIG. 2. Schematic representation of the electrolysis cell. This was a closed cell with self-contained catalyst for H_2 and O_2 recombination, and was instrumented to measure cathode resistance and cell temperature and pressure.

and had a Pt basket containing a catalyst in the upper region to recombine the evolved hydrogen and oxygen generated by electrolysis. A valve was set to release at 1.4 bar to ensure safety from explosion, and a temperature-controlled, high-precision pressure sensor monitored cell pressure and enabled termination of electrolysis if the pressure reached 1.4 bar. The measured pressure was very stable throughout the experiments, indicating that the catalyst performed well.

The electrolyte was composed of either 18 MΩ H₂O containing 0.1 M LiOH or 98+ at. % D₂O with 0.1 M LiOD. Thermocouples measured the electrolyte temperature and the temperature of the x-ray cabinet at 5 different positions. Input electrolysis power to the cells varied but never exceeded 14 W. The electrolyte temperature was highly correlated to the input power. The cell electrolyte temperature increased to as much as 51 °C from a starting temperature of 29 °C during experiments due to this heat source.

Electrolysis was begun using 0.2 to 1.2 mA/cm² current density under current control and required a starting voltage of about 2.2 V to drive the current. The voltage steadily increased with the degree of loading as the chemical potential of the PdH system increases with loading. The degree of loading was estimated using the resistance ratio R/R₀ calibration curves for H or D shown in Fig. 3. Spectra were collected during ~5-min intervals. The error in the R/R₀ measurement is estimated to be <1%.

However, the Pd resistance changed during a run from factors other than just hydrogen content, such as changes in dislocation density, grain size, and lattice strain, so that when the resistance ratio peak is retraced, the maximum can unpredictably change by as much as 6%. Therefore, the R/R₀ measurement is considered a semi-quantitative *in-situ* indicator of loading of the foil. Additionally, R₀ was always measured at room temperature, but the temperature upon reaching the peak in resistance was always higher due to the input power into the cell. Therefore, the peak value of R was temperature corrected to room temperature prior to forming the R/R₀ ratio, using a temperature coefficient of resistance

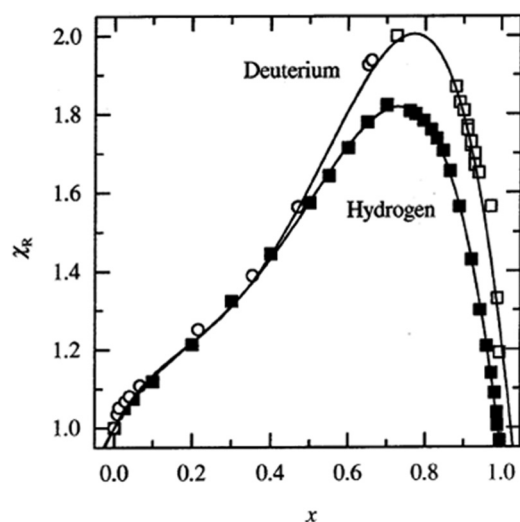


FIG. 3. Resistance ratio R/R₀ or χ_R versus H(D)/Pd ratio x . Data taken from Zhang *et al.*,¹⁶ and references therein. Data were digitized and then fit using fifth order polynomials.

value of 0.004 K⁻¹ taken from the value for pure Pd. Nevertheless, the peak value of the R/R₀ ratio generally differed from literature values (1.8 for H and 2.0 for D), due to extraneous factors as mentioned above. Consequently, the peak value was scaled to the literature value by multiplying R₀ by an appropriate factor.

When R/R₀ approached the peak in Fig. 3, the current was increased in stages to produce a higher loading ratio. At appropriate times when the loading stalled, either the current was increased, or the current set to zero for several minutes and then restarted at a current 20% greater than prior to shutting off the current. These procedures sometimes resulted in a new surface condition where the loading would increase.

Due to the large lattice expansion of Pd when it is loaded with hydrogen (up to 5% lattice parameter increase, 16% volume increase), the cathode began to warp and move immediately upon initiation of electrolysis. This required continuous use of the x-y-z stage and ω to reengage the cathode, since it moved as much as 2 mm as it adjusted to the strain from loading. The problem was less acute at high loadings due to the slower change in H/Pd value and lattice constant with time. The problem was so severe that little data were taken at low loading ratios. In the last run with H₂O, the cathode was deloaded in steps by lowering the current systematically so that some x-ray spectra could be taken at smaller H/Pd ratios.

During each run, additional x-ray fluorescence lines appeared in the spectra that were identified as Sn and Pb. The origin of these impurities was most likely from solder used in wire connections to the feed-through at the top of the cell. Conceptually, the solder dissolved in vapor condensed onto the solder, then dripped back into the electrolyte. The surface of the cathode became coated with impurities from the electrolyte, because metallic ions in the electrolyte will plate out on the cathode during electrolysis. This was confirmed by visual observation of the cathode when the cathodic current was removed. Immediately a cloud of material came off of the cathode turning the electrolyte black in color. Then, the electrolyte cleared in only a few seconds as the material dissolved back into the strong base.

Four cathodes prepared at ENEA were run in the cell. Details of their preparation are described elsewhere.¹⁷ Briefly, cathodes of 0.9995 purity were rolled to 50- μ m thickness, annealed at 900 °C for 8 h, etched in Aqua Regia, and recleaned with alcohol and DI water just prior to insertion into the cell. In one case, a cathode (B) was reused with another batch of electrolyte, after first deloading and recleaning.

All x-ray spectra were least-squares-error fit to obtain peak positions, widths, and intensities. These were analyzed to obtain d spacings and hkl values, then lattice parameter a . At the beginning of loading, few diffraction peaks were found, consistent with few grains being sampled, and the Bragg diffraction condition not readily being satisfied. As the loading progressed, more peaks were observed, consistent with subgrains being formed due to the large lattice strains generated by the hydrogen loading of Pd. In many cases, a single lattice parameter could match all the diffraction peaks observed. However, in some cases, the loading

TABLE I. Cathode loading descriptions.

Cathode	Electrolyte LiOD(H) in	R_0 (m Ω)	Time (h:min)	Charge (C)	Energy (kJ)	Maximum	Maximum
						D(H)/Pd	D(H)/Pd
NRL#2	D ₂ O	3.69	46:15	6337	22.14	From R/R ₀	From a
L23	D ₂ O	3.82	30:15	5974	18.32	0.87	0.893
B2	D ₂ O	10.08	48:22	110947	783.24	0.95	0.977
L5	H ₂ O	5.24	09:56	4354	18.19	0.97	0.946

was heterogeneous, typically resulting in pairs of peaks at the same hkl value. In those spectra, we identified two different lattice parameters. The D (H) composition of the cathode in the β phase of PdD_x (PdH_x) was determined from the measured lattice parameter using the 77 K composition versus lattice parameter data from Schirber and Morosin,¹³ combined with an extrapolation of the thermal expansion data of Hemmes, Geerken, and Griessen¹⁸ provided from 10–250 K.

RESULTS AND DISCUSSION

Table I summarizes results for the four cathodes run over a 9-day period. Table I shows that high maximum loadings ($0.86 < \text{H(D)}/\text{Pd} < 0.98$) were obtained from the lattice parameter *a* for all four cathodes; that the thinnest cathodes (with larger R_0) loaded to the highest H(D)/Pd ratios; and that the R/R₀ method slightly underestimated the maximum loading fraction for the D case, but overestimated it for the H case. The discrepancy was about 2%. Fig. 4 shows the current, voltage and power values needed to obtain the minimum R/R₀ for a D loaded cathode, plotted versus the minimum R/R₀. Higher values of all 3 parameters promote

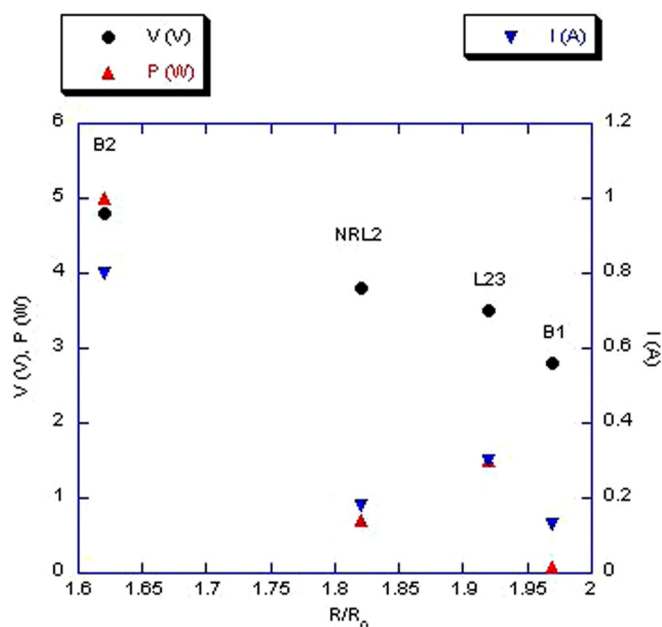


FIG. 4. Cathode operating conditions to obtain the minimum R/R₀ at the highest D loading: current, voltage, and power, versus the minimum R/R₀ obtained.

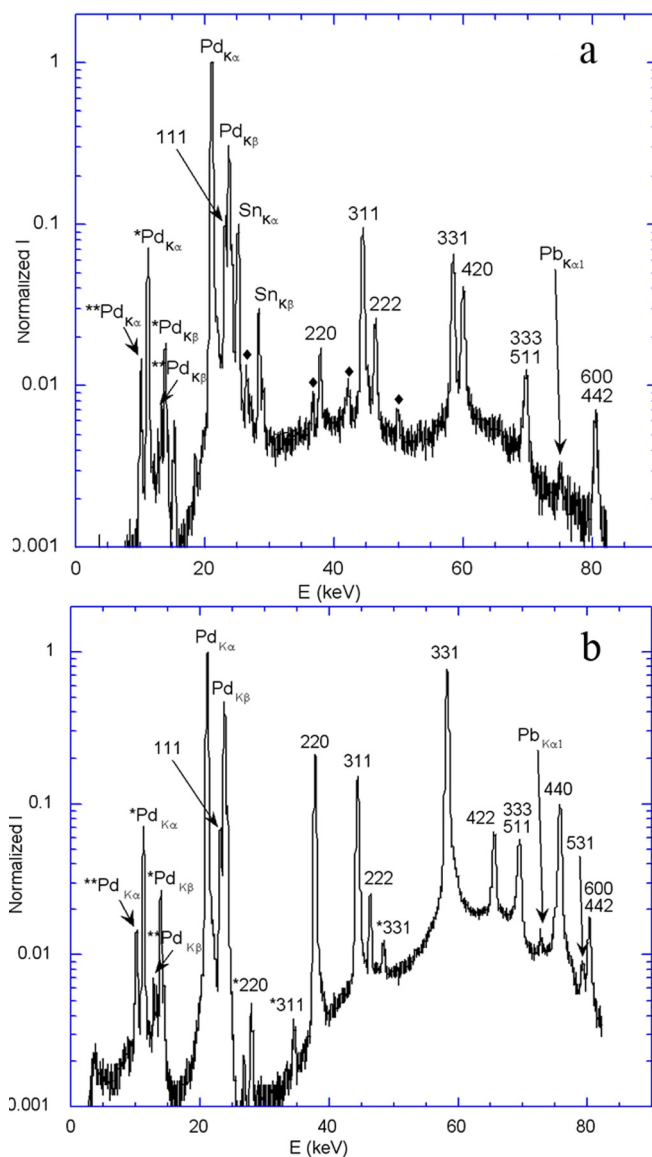


FIG. 5. Typical x-ray diffraction spectra obtained, (a) from cathode B2 (D loaded, spectra 154), and (b) from cathode L5 (H loaded, spectra 229). Besides diffraction peaks marked by their hkl values, there were also fluorescence peaks from Pd, Pb, and sometimes Sn present in spectra, as well as escape peaks caused by escape of Ge_{K α} or Ge_{K β} x rays from the detector (marked by * or **, respectively). Extra diffraction peaks from white Sn deposited on the cathode could sometimes be observed, as indicated by the diamond symbols shown in (a).

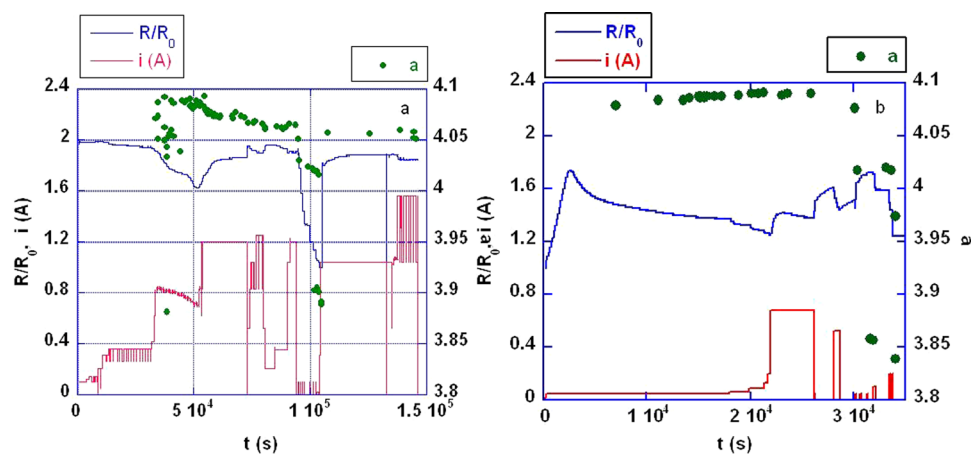


FIG. 6. Time history of (a) cathode B2 loaded with D, and (b) cathode L5 loaded with H. R/R_0 , cell current, and measured lattice parameter a are shown.

better loading, but the strongest correlation is for input power and input current. For all cathodes, higher powers were attempted after the minimum R/R_0 (max. loading) was reached, but the cathodes deloaded and never returned again to the lowest R/R_0 values. For 3 of the 4 cathodes, the electrolyte temperature clearly decreased upon initial loading, caused by the endothermic heat of water hydrolysis combined with the dissolution of D (H) in Pd and the creation of orphan oxygen, preventing their recombination at the catalyst. For the fourth, very low current was initially used so that the thermal signal was below the sensitivity of the measurement.

Figs. 5(a) and 5(b) show x-ray spectra for cathode B2 (D loaded) and cathode L5 (H loaded), respectively. The intensity falls off at low energy due to absorption in electrolyte and at high energy due to x-ray beam intensity fall-off. Diffraction from multiple hkl orientations are identified in the plots, and indicate that the incident x-ray beam intercepted multiple subgrains within the nominal 3 original grains inside the sampled volume. The D/Pd ratio in (a) is 0.913 from the lattice parameter, while R/R_0 indicated a ratio of 0.936 for cathode B2/spectra_154. From (b), the H/Pd ratio is 0.933, which matches the value obtained from R/R_0 for cathode L5/spectra_229. Pd, Sn, and Pb fluorescence peaks are also identified in the spectra, as are satellite escape peaks

from the escape of Ge x rays from the detector, and diffraction peaks likely from Sn deposited on the surface in (a).

Figs. 6(a) and 6(b) display a time history of the lattice constant, R/R_0 , and cell current for cathode B2 (D loaded) and cathode L5 (H loaded), respectively. A general observation is that the deuterium-loaded cathodes displayed variability in the lattice constant upon large current changes (Fig. 6(a), $4E4$ s and $1.0E5$) while the one hydrogen-loaded cathode did not show this variability (Fig. 6(b), $2.2E4$ s). The highest D/Pd ratios occur at the beginning of the electrolysis, and in one case occurred when the R/R_0 ratio had not yet even reached the peak (not shown). A possible explanation is that some orientations of the crystallites have faster kinetics than others and may load to high values unconstrained by neighboring grains. Eventually, the other grains equilibrate, but by then compression prevents all the grains from obtaining the highest value. A second possible explanation is that the Pb and Sn surface impurity build-up over time may reduce the H fugacity and therefore the chemical potential pressure on the surface. This behavior was not observed in the one cathode run with H_2O .

Figs. 7(a) and 7(b) plot the R/R_0 ratio versus lattice constant for cathode B2 and cathode L5, respectively. These data have several features to note. First, there is a very clear delineation between the lattice constants for the α phase

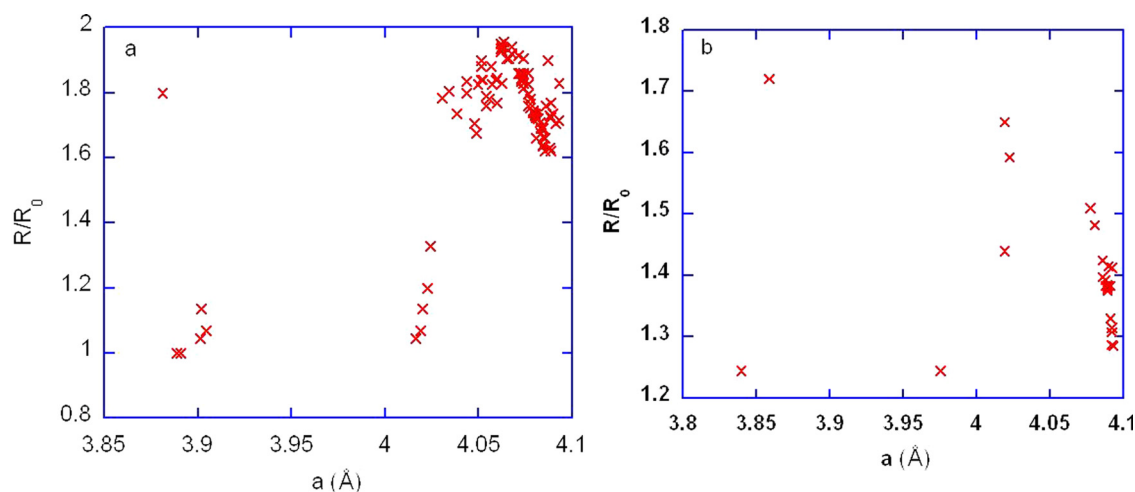


FIG. 7. Comparison of measured R/R_0 with lattice parameter a for (a) cathode B2 loaded with D, and (b) cathode L5 loaded with H.

($a \sim 3.9$) and the β phase ($a > 4$). Second, the collection of data does not appear to follow a smooth curve, especially near the peak in R/R_0 for the B2 cathode. This is largely caused by the heterogeneous loading of subgrains in the Pd foil. While R/R_0 is a bulk average for the foil, XRD was measuring individual subgrains, whose composition varied from subgrain to subgrain during some measurements. In those cases, the diffraction spectra showed multiple peaks for a given hkl for PdD_x , leading to multiple lattice parameters corresponding to the single R/R_0 value. These multiple values of a are plotted in Fig. 7. These cases were most common when the current changed by a large amount.

CONCLUSIONS

For the first time, time resolved, *in-situ*, synchrotron energy-dispersive x-ray diffraction was performed during electrochemical loading of palladium foil cathodes to high levels with hydrogen and deuterium. Concentrations of H/Pd (D/Pd) up to nearly 1 in 0.1M LiOH (LiOD) in H_2O (D_2O) electrolytes were obtained with lattice parameter data monitored throughout the range of concentrations. A number of our observations regarding the electrolysis were consistent with the literature. These include: it is more difficult to load deuterium than hydrogen into palladium, large amounts of impurities are deposited on the cathode from the electrolyte, the *in-situ* relative-resistance measurement of the cathode provides only a semi quantitative guide to the hydrogen concentration, and once a cathode has been loaded to high hydrogen concentration, it is difficult to repeat this high concentration upon subsequent loading. Potential new observations in the electrolysis cell include: higher starting resistivity foils (thinner foils) loaded to higher D concentration, the highest loading fractions occurred during times of large current and/or concentration change, and all 4 cathodes produced at ENEA loaded very well. Observations regarding *in situ* XRD during electrolysis were consistent with the literature in that only the well-known alpha-beta phase transition was observed. New observations from the *in situ* XRD during electrolysis include: data obtained for high D/Pd ratios up to 0.98, the relative resistivity measurement R/R_0 slightly underestimates the XRD measurement of the maximum D/Pd ratio by $\sim 2\%$, there is no obvious new PdD phase at $\text{D/Pd} \sim 1$, and nonuniform loading of hydrogen can occur. Tentative new observations from the XRD data include evidence of rapid loading and deloading (\sim minutes) of the surface while R/R_0 was virtually unchanged, and very few x-ray spectra contained both alpha and beta phases together. This implies that the phase change snaps from Alpha to Beta, and

vice versa, within the time resolution of the data, or about 5 min. The research work demonstrated for the first time with *in situ* XRD that a loading near $\text{D(H)}/\text{Pd} = 1$ may be achieved at room temperature, and can be reasonably controlled.

ACKNOWLEDGMENTS

Use of the National Synchrotron Light Source, Brookhaven National Laboratory, was supported by the U.S. Department of Energy, Office of Science, Office of Basic Energy Sciences, under Contract No. DE-AC02-98CH10886. Additional support was provided by ONR Global for V. Violante travel.

- ¹T. Graham, Proc. R. Soc. London, Ser. A **17**, 212 (1869).
- ²L. Schlapbach and A. Züttel, "Hydrogen storage materials for mobile applications," *Nature* **414**, 353 (2001).
- ³D. Chandra, J. J. Reilly, and R. Chellappa, "Metal hydrides for vehicular applications: The state of the art," *JOM* **58**, 26 (2006).
- ⁴S. Adhikari and S. Fernando, "Hydrogen membrane separation techniques," *Ind. Eng. Chem. Res.* **45**, 875 (2006).
- ⁵J. A. Eastman, L. J. Thompson, and B. J. Kestel, "Narrowing of the palladium-hydrogen miscibility gap in nanocrystalline palladium," *Phys. Rev. B* **48**, 84 (1993).
- ⁶J. K. Jacobs and F. D. Manchester, *J. Less-Common Met.* **49**, 67 (1976).
- ⁷Y. Fukai and N. Ōkuma, "Formation of superabundant vacancies in Pd hydride at high hydrogen pressure," *Phys. Rev. Lett.* **73**, 1640 (1994); S. Miraglia *et al.*, *J. Alloys Compd.* **317**, 77 (2001).
- ⁸D. S. dos Santos, S. Miraglia, and D. Fruchart, *J. Alloys Compd.* **291**, L1 (1999).
- ⁹P. Tripodi *et al.*, "Temperature coefficient of resistivity at compositions approaching PdH," *Phys. Lett. A* **276**, 122 (2000).
- ¹⁰P. Tripodi, D. DiGiacchino, and J. D. Vinko, "Magnetic and transport properties of PdH: Intriguing superconductive observations," *Braz. J. Phys.* **34**, 1177 (2004).
- ¹¹V. F. Rybalko, A. N. Morozov, I. M. Neklyudov, and V. G. Kulish, "Observation of new phases in Pd-D systems," *Phys. Lett. A* **287**, 175 (2001).
- ¹²G. H. Miley, G. Selvaggi, A. Tate, M. Okuniewski, M. Williams, D. Chicea, H. Hora, and J. Kelly, in *Proceedings of the ICCF-8, Villa Marigola, Lerici (La Spezia), Italy* (Italian Physical Society, 2000), p. 169.
- ¹³R. Felici, L. Bertalot, A. DeNinno, A. Labarbera, and V. Violante, "In situ measurement of the deuterium (hydrogen) charging of a palladium electrode during electrolysis by energy dispersive x-ray diffraction," *Rev. Sci. Instrum.* **66**, 3344 (1995).
- ¹⁴E. F. Skelton, P. L. Hagans, S. B. Qadri, D. D. Dominguez, A. C. Ehrlich, and J. Z. Hu, "In situ monitoring of crystallographic changes in Pd induced by diffraction of D," *Phys. Rev. B* **58**, 14775 (1998).
- ¹⁵J. E. Schirber and B. Morosin, *Phys. Rev. B* **12**, 117 (1975).
- ¹⁶W.-S. Zhang, Z.-F. Zhang, and Z.-L. Zhang, *J. Electroanal. Chem.* **528**, 1 (2002).
- ¹⁷V. Violante *et al.*, "Joint scientific advances in condensed matter nuclear science," in 8th International Workshop on Anomalies in Hydrogen/Deuterium Loaded Metals, Sicily, Italy, 2007.
- ¹⁸H. Hemmes, B. A. M. Geerken, and R. Griessen, *J. Phys. F: Met. Phys.* **14**, 2923 (1984).